Photothermal Anti/De-icing Performances of Superhydrophobic Surfaces with Various Micropatterns

ZHANG Haixiang[1*], *ZHU Dongyu*[2], *ZHAO Huanyu*[2], *ZHANG Xiwen*[1], *HE Feng*[1], *HAO Pengfei*[1,3*]

1. School of Aerospace Engineering, Tsinghua University, Beijing 100084, P.R.China;
2. AVIC Aerodynamics Research Institute, Shenyang 110034, P.R.China;
3. Tsinghua University (School of Materials Science and Engineering)-AVIC Aerodynamics Research Institute Joint Research Center for Advanced Materials and Anti/De-icing, Beijing 100084, P.R.China

(Received 25 March 2023; revised 16 April 2023; accepted 26 April 2023)

Abstract: Superhydrophobic photothermal surface shows significant potential in the anti/de-icing field. In this work, we focus on the photothermal anti/de-icing performances of superhydrophobic surfaces with various micropatterns. A finite element simulation, coupling the wave optics and heat transfer models, is employed to illuminate the enhanced photothermal efficiency achieved by the reasonable design of surface micro/nano-structures. The effects of nanoparticle size, volume fraction, and coating thickness on the absorptivity and temperature rise of the photothermal coatings are discussed in detail. Furthermore, two hierarchical textures, including micropillars and microcones, are considered to expound the contribution of micro-scale structures on photothermal performances. Numerical results show that the surface with hierarchical textures has a better absorption efficiency of long waves than the single-scale surface, and the microcones topology presents the best photothermal efficiency. Moreover, the effects of geometric micropattern parameters, e.g. characteristic length and aspect ratio, are also discussed in detail. The illumination and ice melting test demonstrates the efficient anti/de-icing abilities of the superhydrophobic photothermal surfaces prepared in this study. The temperature rise of the optimal structure in this work can reach 45 ℃ under the 1 sun illumination. This work could shed new light on the design optimization of anti/de-icing materials.

Key words: superhydrophobic surface; photothermal; micro patterns; absorptivity; anti/de-icing

CLC number: TN925 **Document code:** A **Article ID:** 1005-1120(2023)02-0137-11

0 Introduction

Freezing on solid surfaces is a common natural phenomenon, which may cause severe safety and economic issues in numerous engineering fields, e.g. aircraft, power transmission lines, cool equipment, wind power generator, etc[1-6]. Hence, significant efforts have been invested in designing active and passive high-efficient anti/de-icing surfaces. Superhydrophobic surfaces (SHSs) have received significant attention thanks to their excellent water repellency and potential icephobic characteristics[7-16].

Numerous studies have demonstrated that SHSs could reduce the liquid-solid contact area and the contact time, and contribute to high-efficiency anti-icing for sessile and impinging drops in supercooled environments due to the micro/nanoscale structures of the SHSs[17-20]. In general, the preferential surface microstructure is regarded as a class of hierarchical textures, including dual-scale and/or triple-scale micro/nanostructures. However, the hierarchical structures can be easily damaged during the ice detachment process, resulting in the decline of hydrophobicity. In addition, once nucleation occurs, SHSs would lose their anti-icing ability due to ice accretion. Hence, fully passive anti-icing has not

*Corresponding authors, E-mail addresses: zhanghx@tsinghua.edu.cn; haopf@tsinghua.edu.cn.

How to cite this article: ZHANG Haixiang, ZHU Dongyu, ZHAO Huanyu, et al. Photothermal anti/de-icing performances of superhydrophobic surfaces with various micropatterns[J]. Transactions of Nanjing University of Aeronautics and Astronautics, 2023, 40(2): 137-147.

http://dx.doi.org/10.16356/j.1005-1120.2023.02.003

been realized, and the durable anti-icing surfaces need to be further studied.

Compared with other active anti/de-icing technologies, e.g. electrothermal technologies, ultrasonic technologies, etc., the photothermal technology uses sunlight without additional power input[21-23]. Therefore, superhydrophobic photothermal surfaces (SPSs) show significant potential in the anti/de-icing field. The combination of the photothermal effect and SHS can simultaneously achieve anti-icing and de-icing abilities[24-26]. Under light conditions, the SHSs can absorb the incident light and transform it into heat energy, resulting in the temperature rise of the photothermal surfaces, which significantly enhances the anti-icing effect of the superhydrophobic surface at low temperatures[27]. Meanwhile, it is possible to spontaneously melt and detach ice without damaging the microstructures under the synergistic action of the photothermal effect and superhydrophobicity.

Inspired by photothermal technology, scholars have performed numerical and experimental studies on the photothermal and anti/de-icing performances of SPSs[27-35]. Wu et al.[36] fabricated hierarchical polydimethylsiloxane (PDMS)/reduced graphene oxide film with high solar energy transfer efficiency and all the frost and glaze could be removed within 300 s under sunlight. Chen et al.[37] produced a durable cauliflower-like micro-nano structured SHS, and the surface exhibits a high absorption rate of 97.3% and a temperature rise of 48.5 ℃ under 1 sun illumination for 300 s. Wang et al.[38-41] employed a multiphysics model that couples electromagnetics and heat transfer to simulate the TiN absorbers using the COMSOL software to better understand the light absorption and light-to-heat conversion mechanisms. Wang et al.[42] adopted a finite difference time domain (FDTD) simulation to illuminate that SiO_2 nanospheres in superhydrophobic layers could enhance the light absorption capacity and guide the designing of SPSs.

In summary, many studies have demonstrated that SPSs show significant potential in the anti/de-icing field and focused on the light-to-heat conversion mechanisms of the nanocoatings. As mentioned above, the hydrophobicity of SHSs usually relies on hierarchical structures, but the effects of the micro/nanostructures on the light-to-heat conversion mechanisms have not been revealed sufficiently. To obtain deeper insights, we investigate the photothermal performances of superhydrophobic surfaces with various micropatterns and focus on the effects of microstructures on light absorption and light-to-heat conversion mechanisms. First, we introduce the numerical and experimental methods in brief. Second, the photothermal properties of nanocoating are discussed in detail. Third, we focus on the effects of hierarchical textures on the photothermal anti/de-icing performances of SHSs and put forward the optimal design of icephobic SPSs.

1 Theory and Method

1.1 Principles of light absorption and heat transfer calculation

We employ COMSOL Multiphysics software to simulate the coupling of electromagnetics and heat transfer and investigate the light absorption and light-to-heat conversion mechanisms[38-39]. The electromagnetic wave and heat transfer in solid and liquid modules are used to represent the electric field and thermal field. The electric field is obtained by solving the time-independent electromagnetic wave equation

$$\nabla \times (\nabla \times \boldsymbol{E}) - k_0^2 \varepsilon_{rc} \boldsymbol{E} = 0 \tag{1}$$

where $\boldsymbol{E}$ is the electric field; k_0 the free space wavenumber; ε_{rc} the space- and wavelength-dependent relative permittivity of the material. The conversion of optical energy to thermal energy can be described as

$$\rho C_p \frac{\partial T}{\partial t} - \nabla \cdot (k \nabla T) = Q_r \tag{2}$$

where T is the temperature and t the time. ρ, C_p, and k are the density, the specific heat capacity, and the thermal conductivity of the considered material, respectively. The generated heat power Q_r can be obtained from

$$Q_r = \frac{\omega \varepsilon_0}{2} \mathrm{Im}(\varepsilon_r) |\boldsymbol{E}|^2 \tag{3}$$

where ω is the angular frequency of the incident light; ε_0 the vacuum permittivity and $\mathrm{Im}(\varepsilon_r)$ the imaginary part of the permittivity.

1.2 Preparation of superhydrophobic photothermal coating

The superhydrophobic photothermal coating

can be fabricated via three steps[38]. First, TiN nanoparticles and PDMS in a certain ratio are added into the ethyl acetate, and the miscible liquids through ultrasonic agitation form a homogeneous solution. Second, the obtained solution is sprayed uniformly onto the substrate using a spray gun. Third, the samples are dried in a draught drying cabinet at 100 ℃ for 2 h. TiN nanoparticles are used here because of their excellent plasmonic properties and photothermal response at visible and near infrared (NIR) regions. The introduction of PDMS could lock the heat transfer near the surface due to its low thermal conductivity and reduce the surface energy of the coating, i.e. render the surface hydrophobic.

1.3 Preparation of hierarchical SPSs

In this work, two kinds of microstructures, micropillars and microcones, are prepared to investigate the photothermal performances on hierarchical SHSs. We fabricate micropillars on silicon surfaces using the standard photolithography technology and etching of inductively coupled plasma (ICP)[43]. The microconed surface is fabricated by the ultrafast laser ablation[44]. The hierarchical SPSs are obtained by spraying the nanocoating on surfaces with microstructures and being dried in a drying chamber for 1 h.

1.4 Illumination, delaying icing and melting ice tests

To investigate their photothermal anti-icing capability, the surfaces are illuminated with a light source that simulates sunlight with light intensity 1 sun = 0.1 W/cm^2. The surface is irradiated with simulated sunlight for 5 min to test intrinsic light-to-heat conversion performance under sunlight. The temperature curves and surface temperature distribution are recorded before and after illumination by a thermal imager. The delaying icing test is also performed. The water drops are placed on the prepared surfaces whose temperature is ranged from 0 ℃ to −20 ℃ by a cold plate, and the delay time of nucleation and icing time of drops on various surfaces are recorded to verify the anti-icing performances of the prepared coatings. Finally, the melting test of prefrozen ice on the surfaces is performed. The water drops are placed on a cold plate and frozen. Then, the surface is irradiated under the simulated sunlight with light intensities of 0.5, 0.8, and 1 sun. The melting test is conducted in a refrigerator, and the ambient humidity and environment temperature are 20% and 0 ℃, respectively. The melting processes are recorded by a thermal imager and a camera.

2 Results and Discussion

2.1 Photothermal properties of nanocoatings

We focus on the photothermal performances of nanocoatings with various particle types, sizes, and volume fractions. The effects of nanoparticle type, size, volume fraction, and coating thickness on the absorptivity and temperature rise of the photothermal coatings are discussed in detail.

2.1.1 Computational models

Fig. 1 shows the geometry and boundary conditions of the photothermal performances of nanocoatings. A plane electromagnetic wave, with a wavelength range from 300—2 500 nm, vertically illumines the substrate with a photothermal nanocoating layer, through the air. The perfect-matched layers (PMLs) are set at the top and bottom of the model to eliminate the effects of boundary reflection. The periodic boundary condition is imposed on the surrounding sides to simulate a nanocoating layer. The particle diameter is d_p, the spacing between two neighboring particles is s_p, and the nanocoating thickness d_n. The intensity of the incident light is 1 sun (0.1 W/cm^2),

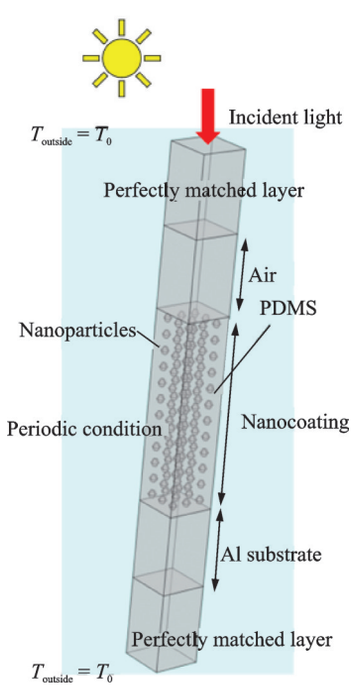

Fig. 1 Modeled geometry and boundary conditions

and the outside temperature is set as $T_0 = 293$ K. The material parameters, including the optical and the thermal parameters, are shown in Table 1.

Table 1 Optical and thermal parameters of the used materials

Material	Density/ (kg•m^{-3})	Thermal conductivity/ (W•(m•K)$^{-1}$)	Specific heat capacity/ (J•(kg•K)$^{-1}$)	Refractive index
Air	1.2	0.024	0.84×10^3	1
TiN	5.4×10^3	60	0.533×10^3	Ref.[45]
PDMS	0.97×10^3	0.16	0.796×10^3	1.4
Al	2.7×10^3	237	0.88×10^3	1.67

2.1.2 Light absorption and light-to-heat conversion

Figs. 2(a, b) illustrate the distribution of electric field intensity and power dissipation density under different illumination wavelengths. It is observed that the wavelength has a great influence on the dissipation of light waves inner the coating. The electric field intensity gradually decreases in the upper layers of the coatings under high-frequency waves (λ = 300 and 500 nm), i.e. the photothermal conversion process occurs. The distribution of electric power dissipation density also indicates that

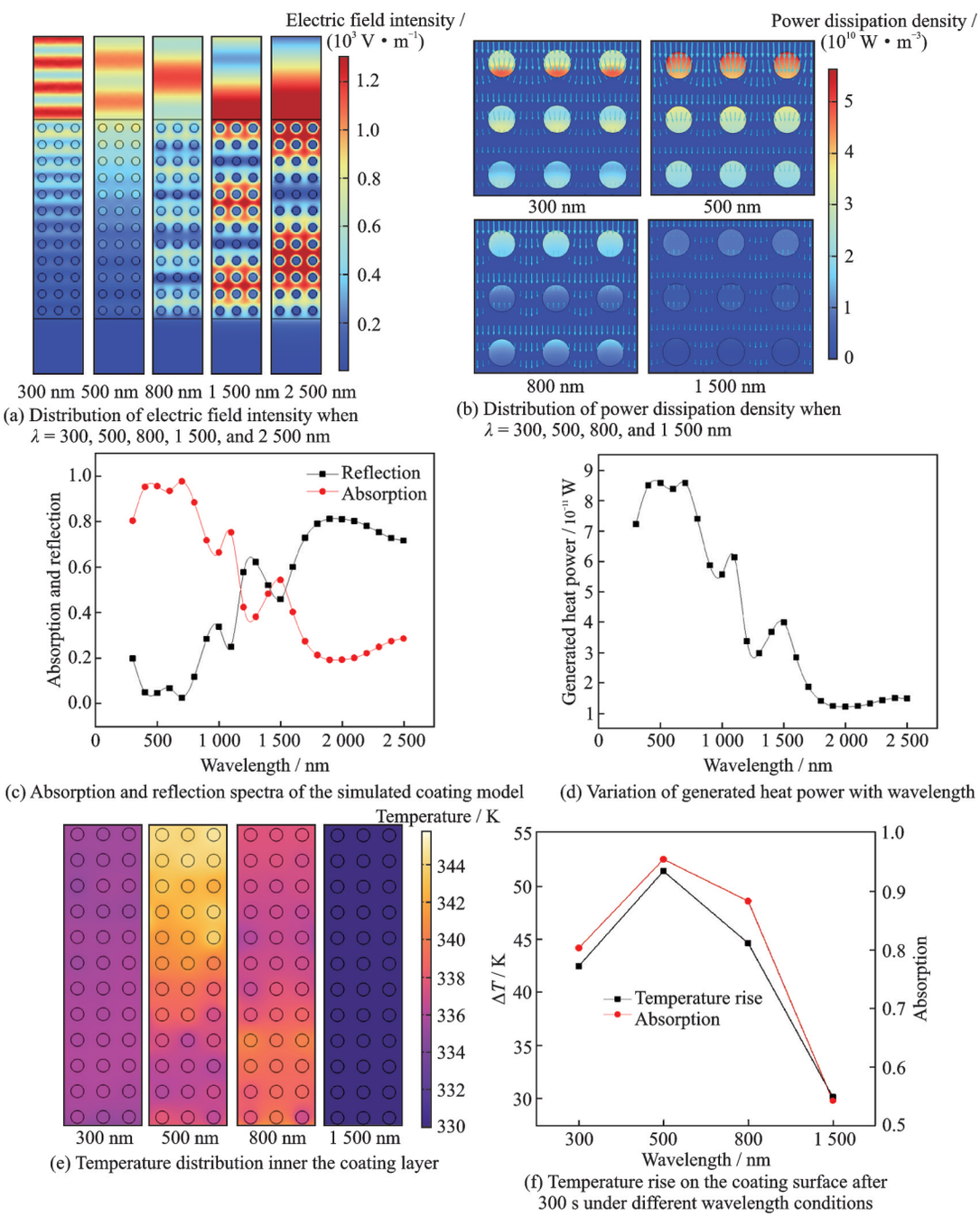

(a) Distribution of electric field intensity when λ = 300, 500, 800, 1 500, and 2 500 nm

(b) Distribution of power dissipation density when λ = 300, 500, 800, and 1 500 nm

(c) Absorption and reflection spectra of the simulated coating model

(d) Variation of generated heat power with wavelength

(e) Temperature distribution inner the coating layer

(f) Temperature rise on the coating surface after 300 s under different wavelength conditions

Fig.2 Optical and light-to-heat conversion properties of the simulated coating model

the top layer of the TiN nanoparticles actively absorbs the incident optical power under high-frequency waves.

Fig. 2(b) shows the absorption and reflection spectra of the simulated model. The absorption (A) can be calculated by $A = 1 - T - R$, where T and R are the transmission and the reflection, respectively (here $T = 0$)[39, 41]. It can be seen from Fig. 2(c) that the simulated coating is good at absorbing optical radiation for short-wavelength waves ($A > 50\%$ when $\lambda < 1\,000$ nm) but holds a terrible absorbing ability for long-wavelength waves ($A > 50\%$ when $\lambda > 1\,000$ nm). Besides, the corresponding curve of generated heat power is consistent with the absorption curve, as shown in Fig. 2(d), indicating that high light absorption is an essential step for efficient photothermal conversion and further be used for anti/de-icing.

The temperature distribution inner the coating layer and the temperature rise on the coating surface after 300 s are shown in Figs. 2(e) and (f), respectively. Similarly, the temperature rise is also consistent with the absorption rate, and the surface temperature can be raised to 53 ℃ when the wavelength $\lambda = 500$ nm. In particular, the temperature increase of the coating is not only related to the light absorption but also depends on the thermal properties of the surrounding medium. Due to the adiabatic properties of the PDMS medium, the generated heat power can be locked inner the coating layer, which is helpful for anti/de-icing.

2.1.3 Effects of nanocoating parameters

In this part, we focus on the effects of nanocoating parameters on light absorption and light-to-heat conversion, and the results could guide the design of photothermal nanocoatings. Fig. 3 shows the absorption spectra and surface temperature statistics of nanocoating models with various layer thicknesses d_n (Figs. 3(a,b)), nanoparticle volume fractions (Figs. 3(c,d)), and nanoparticle diameters d_p (Figs. 3(e,f)).

Comparing Fig. 3(a) with Fig. 3(b), we find that although the absorption rate remains nearly constant, the surface temperature increases with the coating thickness. As mentioned above, the light-to-heat conversion is not only related to light absorption but also to the heat transfer characteristics of the surrounding medium. Due to the low thermal conductivity of the PDMS medium, the increase in coating thickness results in the excellent ability of thermal isolation of the coating.

The proportion of nanoparticles in the coating significantly affects light absorption and light-to-heat conversion. In the visible spectrum, with the increase in nanoparticle volume fraction, the surface temperature rises at first and then tends to a stable

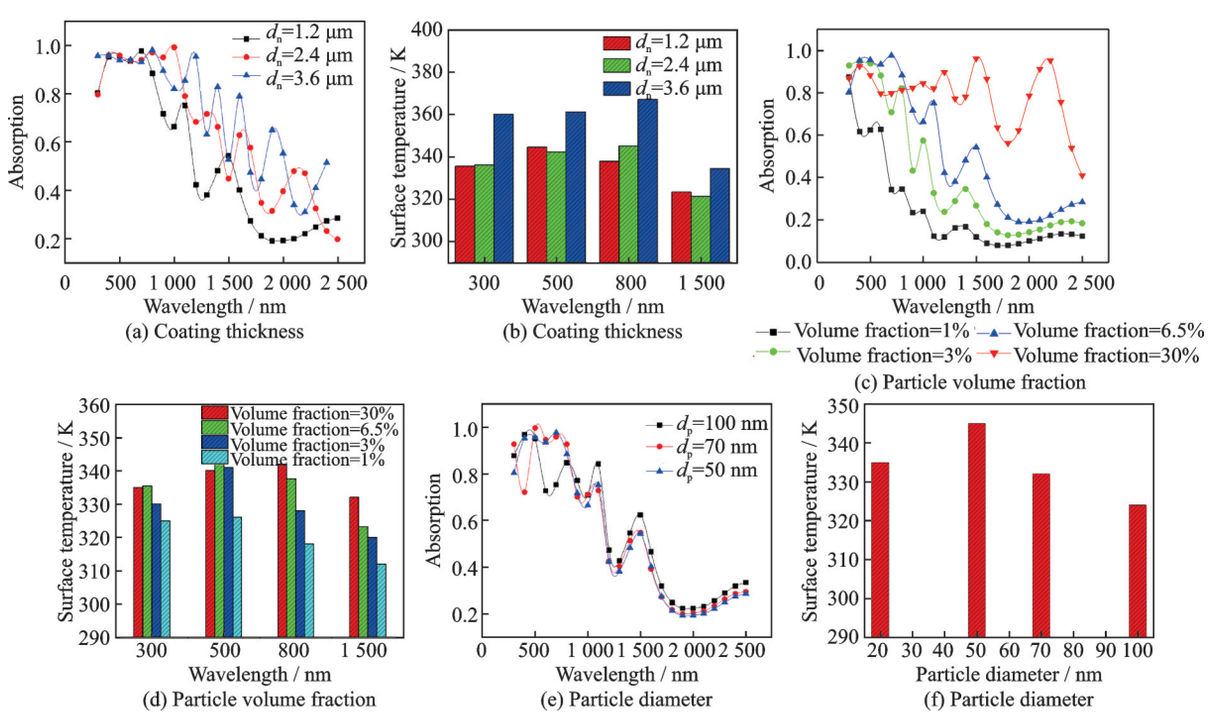

Fig. 3 Influences of nanocoating parameters on light absorption and surface temperature

value. Fig.3(d) shows that the surface temperature is almost the same when the volume fraction is 6% and 30% for wavelength λ = 300 and 500 nm. However, for the long-wavelength band, increasing the volume fraction of nanoparticles can effectively improve the absorption rate and light-to-heat conversion (Fig.3(d) when the wavelength λ = 800 and 1 500 nm). Furthermore, we investigate the effects of particle diameter on photothermal performances. Comparing the three particle sizes used in the numerical simulation (d_p = 50, 70, and 100 nm), one can find that the particle size has a slight influence on light absorption and light-to-heat conversion. The smaller particle size shows slightly better photothermal performances.

2.2 Photothermal properties of hierarchical textures

2.2.1 Computational models

We consider two hierarchical structures, i.e. micropillars, and microcones, to investigate the effect of micropatterns on photothermal performances. Because of the increase in the physical model size, a two-dimensional model is used to save computing resources. Fig.4 shows the geometric models and boundary conditions of the two hierarchical structures. Similar to the boundary conditions in Fig.1, a plane electromagnetic wave, with a wavelength range from 300—2 000 nm, vertically illumines the substrate with hierarchical structures and nanocoating. The PMLs are set at the top and bottom of the model to eliminate the effects of boundary reflection. The periodic boundary condition is imposed on the surrounding sides to simulate microstructure arrays. The thickness of the nanocoatings is set as 0.5 μm, and the length and the height of the microstructures are D and H, respectively. The intensity of the incident light is 1 sun (0.1 W/cm^2), and the outside temperature is set as T_0 = 293 K. The material parameters, including optical and thermal parameters, are shown in Table 1.

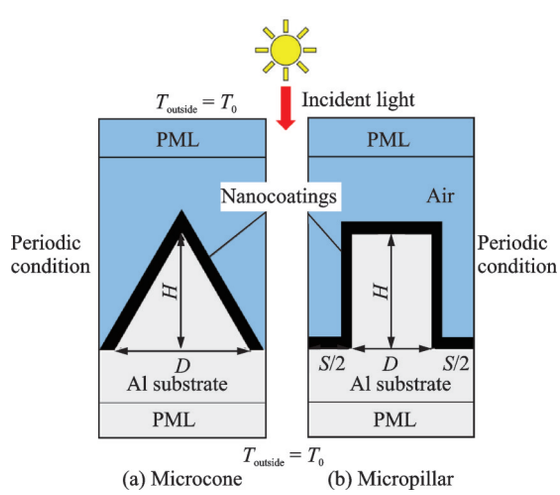

Fig.4 Geometric models and boundary conditions of two hierarchical structures: Microcone and Micropillar

2.2.2 Effects of micro-pattern parameters

In this part, we discuss the influence of the geometric parameters of the microstructures on the photothermal properties. Figs.5(a,b) show the absorption and reflection spectrograms of the involved two models, respectively. The addition of hierarchical structures can promote the light absorption of the long-wavelength wave. Besides, the microcone structure presents the best light absorption characteristics.

The insets in Fig.5 show the distribution of electric field intensity when λ = 500 nm. The elec-

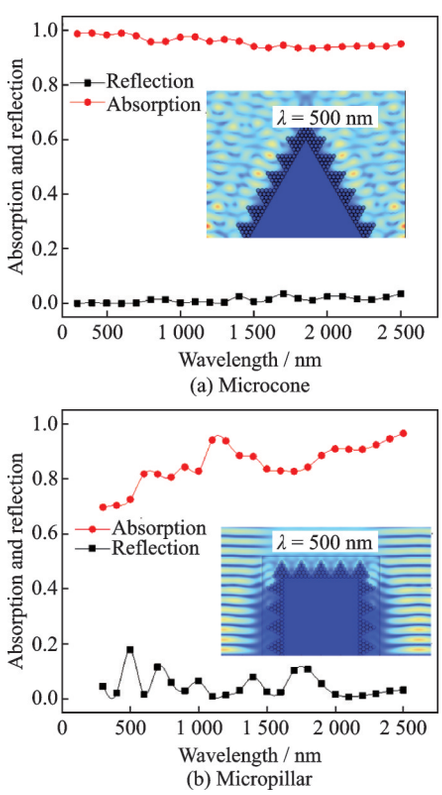

Fig.5 Absorption and reflection spectrograms of the involved two models: Microcone and Micropillar

tromagnetic waves are confined to the gaps of the microcone structures. Light absorption is mainly related to light capture and light limitation, when the electromagnetic wave reaches the inside of the microstructures. The electromagnetic waves are confined to resonating within the structure and are consumed to generate heat power.

Fig.6(a) shows the influence of the characteristic size of the micropillars on the light absorption rate and temperature rise of the substrate for the wavelength $\lambda = 500$ nm. Here, we define the dimensionless parameter D/λ, representing the ratio of microstructure characteristic length to wavelength. With the increase of the dimensionless parameter D/λ, the absorption and temperature rise approach a constant value. When the microstructure characteristic length is on the same order of magnitude as wavelength, the light absorption, and temperature can reach the maximum value, which is significantly meaningful for designing photothermal surfaces. Fig.6(b) shows the surface temperature statics under different aspect ratios of the microcones for the wavelength $\lambda = 500$ nm, and the surface temperature increases with the aspect ratio of the microcones. In other words, the rough structures help to capture and limit electromagnetic waves and lead to higher absorption. This result provides a guiding idea for designing efficient photothermal surfaces.

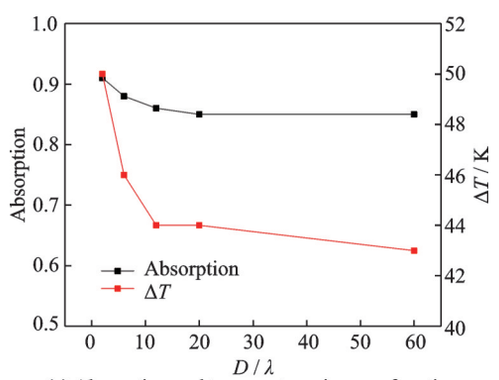

(a) Absorption and temperature rise as a function of the defined dimensionless parameter D/λ

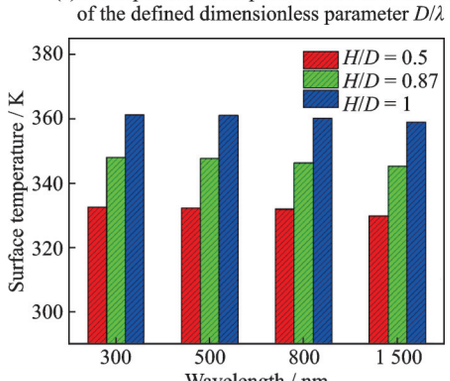

(b) Surface temperature statics under different aspect ratios of the microcone

Fig.6 Influences of geometrical parameters on light absorption and light-to-heat conversion with the wavelength $\lambda = 500$ nm

2.3 Experimental results

Based on the simulation results in Section 2.1, we prepare the photothermal coating and conduct the illumination test on different substrates and the ice melting experiment. Detailed experimental procedures have been introduced in Sections 1.3 and 1.4. The microscopic morphologies of superhydrophobic photothermal surfaces prepared in this study are shown in Fig.7. The apparent contact angle and the contact angle hysteresis on these substrates are measured from water drops of 5 μL using a standard contact angle goniometer (JC2000CD1, POWEREACH) and shown in Table 2.

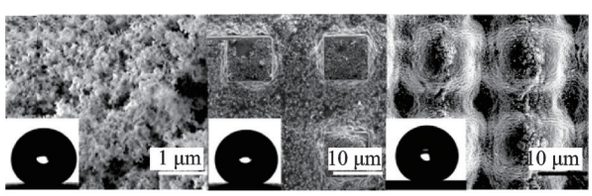

(a) Nanocoating (b) Micropillars (c) Microcones

Fig.7 SEM images of SPSs prepared in this study

Table 2 Wetting properties of SPSs in this study

Substrate	Contact angle/(°)	Contact angle hysteresis/(°)
Smooth	150 ± 3	9 ± 0.5
Micropillar	149 ± 3	12 ± 3.5
Microcone	158 ± 4	7 ± 2

2.3.1 Illumination test

Three kinds of substrates, including a smooth aluminum base, a silicon wafer with micropillars, and an aluminum base with microcones, are selected to conduct the illumination test. The intensity of the incident light is 1 sun (0.1 W/cm^2). Fig.8 shows the surface temperature versus time (Fig.8(a)) and the distribution of surface temperature (Fig.8(b)) of the three substrates within 5 min at 1 sun incident light at the room temperature. For the smooth aluminum

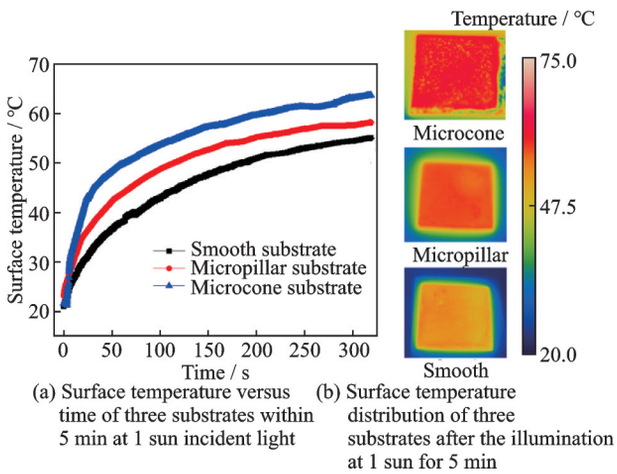

(a) Surface temperature versus time of three substrates within 5 min at 1 sun incident light (b) Surface temperature distribution of three substrates after the illumination at 1 sun for 5 min

Fig.8 Photothermal properties of different substrates

substrate without microstructures, the surface temperature can rise to 53 ℃ only relying on the nanocoatings. For the micropillar structures, the photothermal effect is slightly increased, and the surface temperature can rise to 58 ℃. In particular, the surface temperature can reach 64 ℃ (the temperature increase is about 45 ℃) on the aluminum base with microcones. The experimental results show that the microcone structure has stronger light absorption and photothermal conversion ability.

2.3.2 Delaying icing test

As described in Section 1.4, we also perform the delaying icing test to verify the anti-icing performances of the prepared surfaces. The delay time of nucleation t_{delay} and icing time of drops t_{icing} on various surfaces are listed in Table 3. The delay time of nucleation refers to the duration from cooling to nucleation, and the icing time refers to the duration during the freezing process.

Table 3 t_{delay} and t_{icing} on various surfaces s

Parameter	Smooth-Al	Nanocoating	Micropillar	Microcone
t_{delay}	53	90	95	600
t_{icing}	6	51	48	50

Here, a smooth aluminum base is employed as a contrastive surface to compare the delaying icing effects of the prepared surfaces in this study. As shown in Table 3, the surface with nanocoating in this work has an excellent anti-icing performance. The delay time of nucleation on the nanocoating surface can be delayed to be two times compared with the smooth aluminum base. Especially, the microconed surface can delay the nucleation time to 600 s. The icing time of drops on SPSs can be delayed eight times compared with the smooth aluminum base.

2.3.3 Ice melting test

In addition, the ice melting test is also conducted on micropillar substrates under a supercooled environment. Figs.9(a,b) show the images and corresponding temperature distribution of the ice melting process. In the ice melting experiment, the ice particle is priorly frozen by putting a water drop on a clod substrate at −20 ℃. Then the temperature of the cold plate is kept at −5 ℃, and an incident light with an intensity of 0.5, 0.8 and 1 sun illuminates the substrate. The ambient humidity and the environment temperature are kept at 20% and 0 ℃, respectively.

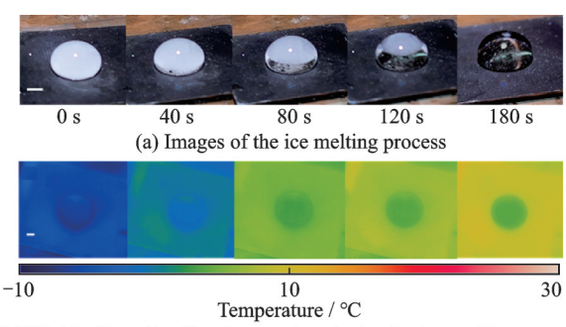

(a) Images of the ice melting process

(b) Distribution of surface temperature during the ice melting process

Fig.9 Ice melting process on a SPSs with micropillar structures under 1 sun condition

As shown in Fig.9, with the passage of illumination time, the surface temperature gradually increases accompanied by the ice melting. It takes 180 s for the ice particle to melt, and the surface temperature can rise to 10 ℃. The ice-melting experiment also verified the practicability of the photothermal surface prepared in this study.

Since the sunlight intensity in winter is far less than 1 sun, the effects of light intensity on ice melting are also investigated. The melting time of the ice particle under different light intensities is shown in Fig.10. The melting time increases with the reduction of the inclined light intensity. The ice particle can be effectively melted just under a light intensity of 0.5 sun.

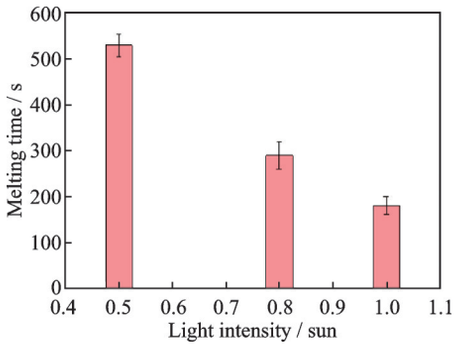

Fig.10 Melting time under different light intensities

3 Conclusions

We investigate the photothermal anti/de-icing performances of SHSs with various micropatterns. The effects of nanoparticle size, volume fraction, and coating thickness on the absorptivity and temperature rise of the photothermal coatings are discussed in detail. The increase of nanocoating thickness and nanoparticle volume fraction can effectively promote light absorption and light-to-heat conversion. Especially, for the long-wavelength band, increasing the volume fraction of nanoparticles can effectively improve the absorption rate and the light-to-heat conversion. Two hierarchical textures, micropillars and microcones, are considered to expound the contribution of micro-scale structures on photothermal performances. The addition of hierarchical structures can promote the light absorption of the long-wavelength wave, and the microcone structure presents the best light absorption characteristics. Moreover, the effects of geometric micropattern parameters, e.g. characteristic length and aspect ratio, are also discussed in detail. It is found that when the microstructure characteristic length is on the same order with the wavelength, the light absorption and temperature can reach the maximum value, which is significantly meaningful for designing photothermal surfaces. Besides, the increase of surface roughness also helps to capture and limit electromagnetic waves and leads to higher absorption. The illumination test demonstrates the microcone substrates hold on the best photothermal performances, which is consistent with the numerical results. The temperature rise of the microcone substrates in this work can reach 45 ℃ under the 1 sun illumination. The experimental results show the surfaces prepared in this work present an excellent anti/de-icing performances. We believe that this work helps to provide feasible strategies for photothermal SHSs fabrication. Furthermore, based on this study, there are still a lot of tasks to explore, e.g. the ice-melting efficiency of photothermal SHSs on different microstructural surfaces and coating stability. We will continue to do further in-depth studies in future.

References

[1] SHEN Y, WU X, TAO J, et al. Icephobic materials: Fundamentals, performance evaluation, and applications[J]. Progress in Materials Science, 2019, 103(1): 509-557.

[2] ROISMAN I V, TROPEA C. Wetting and icing of surfaces[J]. Current Opinion in Colloid & Interface Science, 2021, 53(1): 101400.

[3] JUNG S, TIWARI M K, DOAN N V, et al. Mechanism of supercooled droplet freezing on surfaces[J]. Nature Communications, 2012, 3(1): 615.

[4] ZHUO Y, XIAO S, AMIRFAZLI A, et al. Polysiloxane as icephobic materials—The past, present and the future[J]. Chemical Engineering Journal, 2021, 405: 127088.

[5] ZHAO G, ZOU G, WANG W, et al. Competing effects between condensation and self-removal of water droplets determine antifrosting performance of superhydrophobic surfaces[J]. ACS Applied Materials Interfaces, 2020, 12(6): 7805-7814.

[6] NATH S, AHMADI S F, BOREYKO J B. A review of condensation frosting[J]. Nanoscale and Microscale Thermophysical Engineering, 2016, 21(2): 81-101.

[7] WANG P, LI Z, XIE Q, et al. A passive anti-icing strategy based on a superhydrophobic mesh with extremely low ice adhesion strength[J]. Journal of Bionic Engineering, 2021, 18(1): 55-64.

[8] JEEVAHAN J, CHANDRASEKARAN M, BRITTO J G, et al. Superhydrophobic surfaces: A review on fundamentals, applications, and challenges[J]. Journal of Coatings Technology and Research, 2018, 15(2): 231-250.

[9] BOINOVICH L B, EMELYANENKO K A, EMELYANENKO A M. Superhydrophobic versus SLIPS: Temperature dependence and the stability of ice adhesion strength[J]. Journal of Colloid Interface Science, 2022, 606(1): 556-566.

[10] HE Y, JIANG C, CAO X, et al. Reducing ice adhesion by hierarchical micro-nano-pillars[J]. Applied Surface Science, 2014, 305(1): 589-595.

[11] WANG Y, HUANG J T. Large-scale fabrication of graded convex structure for superhydrophobic coating inspired by nature[J]. Materials (Basel), 2022, 15(6): 2179.

[12] SARKAR D K, FARZANEH M. Superhydrophobic coatings with reduced ice adhesion[J]. Journal of Adhesion Science and Technology, 2009, 23(9): 1215-1237.

[13] RABBANI S, BAKHSHANDEH E, JAFARI R, et al. Superhydrophobic and icephobic polyurethane coatings: Fundamentals, progress, challenges and opportunities[J]. Progress in Organic Coatings, 2022, 165(1): 106715.

[14] ZHAO G, ZOU G, WANG W, et al. Rationally designed surface microstructural features for enhanced droplet jumping and anti-frosting performance[J]. Soft Matter, 2020, 16(18): 4462-4476.

[15] WANG F, ZHUO Y, HE Z, et al. Dynamic anti-icing surfaces (DAIS)[J]. Advanceal Science (Weinh), 2021, 8(21): e2101163.

[16] WANG D, SUN Q, HOKKANEN M J, et al. Design of robust superhydrophobic surfaces[J]. Nature, 2020, 582(7810): 55-59.

[17] VERCILLO V, TONNICCHIA S, ROMANO J M, et al. Design rules for laser-treated icephobic metallic surfaces for aeronautic applications[J].Advanced Functional Materials, 2020, 30(16): 1910268.

[18] WANG F, LV F, LIU Y, et al. Ice adhesion on different microstructure superhydrophobic aluminum surfaces[J]. Journal of Adhesion Science and Technology, 2013, 27(1): 58-67.

[19] WANG L, GONG Q, ZHAN S, et al. Robust anti-icing performance of a flexible superhydrophobic surface[J]. Advanced Materials, 2016, 28(35): 7729-7735.

[20] JIANG Y, CHOI C H. Droplet retention on superhydrophobic surfaces: A critical review[J]. Advanced Materials Interfaces, 2020, 8(2): 2001205.

[21] YANG H, WANG Z, TAN S, et al. Bio-inspired anti-icing material as an energy-saving design toward sustainable ice repellency[J]. Advanced Materials Technologies, 2022(1): 2200502.

[22] YILBAS B S, KELES O, TOPRAKLI A Y. Surface engineering towards self-cleaning applications: laser textured silicon surface[J]. Procedia Engineering, 2017, 184(1): 716-724.

[23] WANG W, CAI Y, DU M, et al. Ultralight and flexible carbon foam-based phase change composites with high latent-heat capacity and photothermal conversion capability[J]. ACS Applied Materials Interfaces, 2019, 11(35): 31997-32007.

[24] LI R, YANG L, ZHOU C, et al. Fast self-healing superhydrophobic sponge with all-weather heating and anti-fouling properties[J]. Materials Today Chemistry, 2022, 23(1): 100730.

[25] GUO W, LIU C, LI N, et al. A highly transparent and photothermal composite coating for effective anti-/de-icing of glass surfaces[J]. Nanoscale Advances, 2022, 4(13): 2884-2892.

[26] WANG P, WANG J, DUAN W, et al. A superhydrophobic/electrothermal/photothermal synergistically anti-icing strategy with excellent self-healable and anti-abrasion property[J]. Journal of Bionic Engineering, 2021, 18(5): 1147-1156.

[27] MA W, LI Y, YAO S H, et al. Recent advances in solar-thermal surfaces for anti-icing/anti-frosting/anti-fogging[J]. Acta Physica Sinica, 2022, 71(8): 089201.

[28] LI H, LI Y, WU J, et al. Bio-inspired hollow carbon microtubes for multifunctional photothermal protective coatings[J]. ACS Applied Materials Interfaces, 2022, 14(25): 29302-29314.

[29] LI N, ZHANG Y, ZHI H, et al. Micro/nano-cactus structured aluminium with superhydrophobicity and plasmon-enhanced photothermal trap for icephobicity[J]. Chemical Engineering Journal, 2022, 429(1): 132183.

[30] CHENG S, GUO P, WANG X, et al. Photothermal slippery surface showing rapid self-repairing and exceptional anti-icing/deicing property[J]. Chemical Engineering Journal, 2022, 431(1): 133411.

[31] LI Y, MA W, KWON Y S, et al. Solar deicing nanocoatings adaptive to overhead power lines[J]. Advanced Functional Materials, 2022, 32(25): 2113297.

[32] LU H, SHI H, SATHASIVAM S, et al. Strong robust superhydrophobic C/silicone monolith for photothermal ice removal[J]. Journal of Materials Science, 2022, 57(13): 6963-6970.

[33] YU B, SUN Z, LIU Y, et al. Improving anti-icing and de-icing performances via thermal-regulation with macroporous xerogel[J]. ACS Applied Materials Interfaces, 2021, 13(31): 37609-37616.

[34] JIANG G, LIU Z, HU J. Superhydrophobic and photothermal PVDF/CNTs durable composite coatings for passive anti-icing/active de-icing[J]. Advanced Materials Interfaces, 2021, 9(2): 2101704.

[35] JIANG G, CHEN L, ZHANG S, et al. Superhydrophobic SiC/CNTs coatings with photothermal deicing and passive anti-icing properties[J]. ACS Applied Materials Interfaces, 2018, 10(42): 36505-36511.

[36] WU B, CUI X, JIANG H, et al. A superhydrophobic coating harvesting mechanical robustness, passive anti-icing and active de-icing performances[J]. Journal of Colloid Interface Sciences, 2021, 590(1): 301-310.

[37] CHEN C, TIAN Z, LUO X, et al. Cauliflower-like micro-nano structured superhydrophobic surfaces for

durable anti-icing and photothermal de-icing[J]. Chemical Engineering Journal, 2022, 450(1): 137936.
[38] WANG B, JING Z, ZHAO M, et al. Ultraflexible photothermal superhydrophobic coating with multifunctional applications based on plasmonic tin nanoparticles[J]. Advanced Optical Materials, 2022, 10(12): 2200168.
[39] WANG B, WANG W, ASHALLEY E, et al. Broadband refractory plasmonic absorber without refractory metals for solar energy conversion[J]. Journal of Physics D: Applied Physics, 2020, 54(9): 094001.
[40] WANG B, YU P, WANG W, et al. High-Q plasmonic resonances: Fundamentals and applications[J]. Advanced Optical Materials, 2021, 9(7): 2001520.
[41] WANG B, YU P, YANG Q, et al. Upcycling of biomass waste into photothermal superhydrophobic coating for efficient anti-icing and deicing[J]. Materials Today Physics, 2022, 24(1): 100683.
[42] WANG M, YANG T, CAO G, et al. Simulation-guided construction of solar thermal coating with enhanced light absorption capacity for effective icephobicity[J]. Chemical Engineering Journal, 2021, 408(1): 127316.
[43] ZHANG H, ZHANG X, HE F, et al. How micropatterns affect the anti-icing performance of superhydrophobic surfaces[J]. International Journal of Heat and Mass Transfer, 2022, 195123196.
[44] WANG L, TIAN Z, JIANG G, et al. Spontaneous dewetting transitions of droplets during icing & melting cycle[J]. Nature Communications, 2022, 13(1): 378.
[45] PFLÜGER J, FINK J, WEBER W, et al. Dielectric properties of TiC_x, TiN_x, VC_x, and VN_x from 1.5 to 40 eV determined by electron-energy-loss spectroscopy[J]. Physical Review B, 1984, 30(3): 1155-1163.

Acknowledgements This work was supported by the National Natural Science Foundation of China (Nos. 11972215, 12072174, 12172189, 52111540269), the National Key R&D Program of China (Nos.2022YFC2402600, 2018FYA0305800), and the China Postdoctoral Science Foundation (No. 2021M701907).

Authors Dr. **ZHANG Haixiang** received the Ph.D. degree in mechanics from Tsinghua University in 2021. Now, he is a postdoctoral fellow at School of Aerospace Engineering, Tsinghua University. His research focuses on drop dynamics and anti/de-icing.

Prof. **HAO Pengfei** received the Ph.D. degree in mechanics from Tsinghua University. Now, he is an associate professor at School of Aerospace Engineering, Tsinghua University. His research focuses on fluid mechanics.

Author contributions Dr. **ZHANG Haixiang** conducted formal analysis, investigation, methodology, and wrote the original draft. Dr. **ZHU Dongyu** conducted funding acquisition, project administration, and managed the resources. Dr. **ZHAO Huanyu** conducted funding acquisition, project administration, and managed the resources. Prof. **ZHANG Xiwen** conducted funding acquisition, validation, visualization, wrote the literature review, and proofread the manuscript. Prof. **HE Feng** contributed to the methodology, managed the resources, and proofread the manuscript. Prof. **HAO Pengfei** conducted funding acquisition and project administration, contributed to the methodology, managed the resources, and proofread the manuscript. All authors commented on the manuscript and draft and approved the submission.

Competing interests The authors declare no competing interests.

(Production Editor: ZHANG Bei)

不同微结构超疏水表面的光热防除冰特性

张海翔[1]，朱东宇[2]，兆环宇[2]，张锡文[1]，何　枫[1]，郝鹏飞[1,3]

(1.清华大学航天航空学院，北京 100084，中国；2.航空工业空气动力研究院，沈阳 110034，中国；
3.清华大学(材料学院)-航空工业气动院先进材料与防除冰技术联合研究中心，北京 100084，中国)

摘要：超疏水光热防除冰表面作为一种新兴的防除冰手段，在防除冰领域具有巨大的应用潜能。本研究通过数值模拟和物理实验相结合的手段研究了不同微结构超疏水表面的光热防除冰特性。基于有限元模拟，得到了纳米颗粒的粒径、种类、体积分数、涂层厚度及微纳复合结构表面的结构参数对表面光热转化效率和升温效果的影响。另外，考虑了微柱和微锥两种微纳复合结构，数值结果表明微纳复合结构具有更好的光热特性，微锥结构的光热特性最好。同时，详细讨论了微结构尺寸参数，如特征尺度和高宽比，对表面吸收率与光热转化效率的影响。光照升温和融冰试验结果表明制备的超疏水光热表面能够实现高效的光热转化和防除冰功能，最优结构的表面在一个太阳光照条件下的温升可以达到45 ℃。本研究的研究工作可以为防除冰材料的优化设计提供参考。

关键词：超疏水表面；光热特性；微结构；吸收率；防除冰